Influence of substrate–film interface engineering on the superconducting properties of $YBa_2Cu_3O_{7-\delta}$

Guus Rijnders,[a] Seve Currás, Mark Huijben, Dave H. A. Blank, and Horst Rogalla
Faculty of Science & Technology, MESA+ Institute for Nanotechnology, University of Twente, The Netherlands

(Received 20 June 2003; accepted 12 December 2003)

The atomic stacking sequence at the substrate–film interface plays an essential role in the heteroepitaxial growth of $REBa_2Cu_3O_{7-\delta}$. During initial growth, the interface configuration influences the surface morphology and structural properties of the film, due to the formation of anti-phase boundaries (APBs) by coalescence of islands with different stacking sequences. In this study, the interface configuration is accurately controlled by both the terminating atomic layer of the $SrTiO_3$ substrate and the stoichiometry of the first unit cell layer. Using this capability the network of APBs and, therefore, the in-plane ordering is tuned, allowing the study of its influence on the structural and electrical properties of the $YBa_2Cu_3O_{7-\delta}$ film. The critical temperature T_c is depressed by increase of the in-plane ordering, which strongly indicates that the presence of APBs in the sample favors the oxygen in-diffusion. © *2004 American Institute of Physics.*
[DOI: 10.1063/1.1646463]

The structural properties, i.e., defect and crystalline structure and surface morphology, of $REBa_2Cu_3O_{7-\delta}$ (RE123) thin films influence their electrical properties, and the applicability of these superconducting cuprates in heteroepitaxial structures is, therefore, hampered. For instance, structural defects, grain boundaries, and antiphase boundaries (APBs) play an important role in flux pinning mechanisms,[1–4] whereas the surface morphology of RE123 thin films is important for multilayer structures, which require smooth surfaces. The structural properties and surface morphology are a direct result of thin film growth, influenced by deposition conditions and substrate properties.

Different deposition techniques are applied for the growth of RE123 thin films, as reactive co-evaporation, molecular beam epitaxy, and pulsed laser deposition (PLD). Independent of the deposition technique used, the growth unit has to satisfy charge neutrality. When all constituents are provided simultaneously, for instance in the case of PLD, the growth unit is the RE123 unit cell. One direct implication of this fact is the requirement of a specific stacking sequence of the individual atomic layers constituting this unit-cell. During the initial stage of growth, the stacking sequence will be influenced by the substrate surface properties, i.e., the terminating atomic layer and its crystalline structure. The first atomic layer and, consequently, the sequence of the initial RE123 unit cell layer will depend on these properties. We reported recently[5] on the stacking sequence at the interface (SSI) of RE123 on single TiO_2-terminated $SrTiO_3$ (STO) substrates. We concluded, from high resolution electron microscopy measurements, that RE123 films grown on TiO_2-terminated STO substrates present a perovskite-like interface with two SSIs: $bulk–SrO–TiO_2–BaO–CuO–BaO–CuO_2–RE–CuO_2–BaO–bulk$ (referred as RE133) and $bulk–SrO–TiO_2–BaO–CuO_2–RE–CuO_2–BaO–bulk$ (referred as RE122).

The coexistence of different SSIs leads to surface roughening and plays an essential role in the formation of APBs oriented perpendicularly to the substrate–film interface. These APBs, which are the most prominent type of defects occurring in ultrathin RE123 films, start at the interface and persist over the total film thickness.[5] Some authors have related such planar defects to unit-cell steps on the substrate.[6] We observed[5] that the density of APBs in RE123 ultrathin films grown on TiO_2-terminated STO is large compared to the density of substrate unit cell steps, indicating that APBs are formed on the atomically smooth terraces due to the coalescence of neighboring islands with different SSIs.

In this letter, we study the influence of the stacking sequence at the substrate–film interface and the related network of APBs on the electrical properties of *c*-axis oriented $YBa_2Cu_3O_{7-\delta}$ (Y123) ultrathin films. We use three different interface configurations in this study (see Fig. 1).

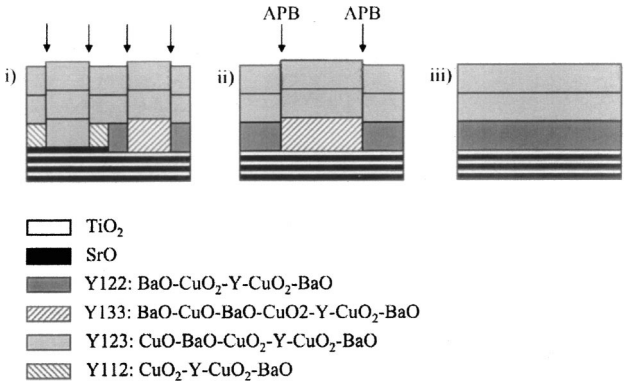

FIG. 1. Schematic representation of the three interface configuration used on growing Y123: (i) on as-received (double-terminated) STO, where four stacking sequences at the interface are possible, (ii) on single TiO_2-terminated STO, allowing two different SSIs, and (iii) on TiO_2-terminated STO using Y122 for the first unit cell layer, giving rise to a stacking sequence in the terraces. In these cases, the coalescence of islands with different stacking sequence causes the formation of antiphase boundaries (indicated by arrows).

[a]Electronic mail: a.j.h.m.rijnders@utwente.nl

(i) Y123 on as-received vicinal STO substrates. The surface of these substrates consists of terraces (average length ~150 nm in the present work) with disordered step ledges and islands on the terraces with height differences of integer numbers of half unit cell (~2 Å). This indicates the coexistence of the two possible surface arrangements:[7] SrO- and TiO_2-terminated domains [in the remainder of the text referred to as (DT) double-terminated]. This will lead to four possible SSIs.

(ii) Y123 on TiO_2-terminated STO substrates. Using the procedure described in Ref. 7, STO substrates are treated in order to get atomically smooth single terminated surfaces. As mentioned before, this will lead to two different SSIs.

(iii) Y123/Y122 on TiO_2-terminated STO substrates. Stoichiometric deposition with a cation ratio Y:Ba:Cu=1:2:2 during growth of the first unit-cell layer leads to the precise control of the interface configuration by suppression of the Y133 configuration. This procedure gives rise to one SSI.

These films, presenting different interface configurations, are deposited by PLD on (100) STO and their growth is *in situ* monitored by reflection high-energy electron diffraction (RHEED), allowing control of the thickness. It is known that the initial pseudomorphic growth mode changes to island growth to release the epitaxial strain over a critical thickness t_c, which scales with the inverse of the lattice mismatch.[8] For Y123 on STO[9] the critical thickness was estimated to be in the range of 15 nm. All the films studied here present thicknesses ranging from 5 to 10 unit cells, which allows study of the influence of the SSI on the superconducting properties without interference from strain relaxation mechanisms.

Concerning the PLD deposition conditions, a sintered ceramic target with the nominal stoichiometry Y:Ba:Cu =1:2:3 is ablated using a KrF-laser (248 nm) with an energy density of 1.3 J cm^{-2}. During growth, the substrate is held at 780 °C in a flow of pure oxygen at 0.1 mbar. Similar temperature and oxygen background pressure conditions are used when depositing the Y122 layer, but the energy density at the target (nominal stoichiometry Y:Ba:Cu=1:2:2) is 7 J cm^{-2}. In this case, pulsed laser interval deposition[10] is used to obtain an atomically smooth single unit-cell layer, followed by *in situ* annealing for 1 h at 830 °C before depositing the Y123. On top of the samples that have been electrically characterized, a protective $SrRuO_3$ layer is grown at 600 °C in an oxygen pressure of 0.13 mbar. Finally, all samples are annealed in an oxygen atmosphere at 700 mbar at 600 °C and then at 450 °C, for 30 min in each plateau.

During deposition, film growth is monitored *in situ* by a RHEED system that can operate at the high oxygen pressures used.[11] In Fig. 2, the RHEED specular intensities recorded during the growth of Y123 layers with the different interface configurations are shown. In case of this SSI, a large recovery of the RHEED intensity is observed during growth of the initial Y122 layer. This and the corresponding RHEED pattern, exhibiting clear two-dimensional (2D) spots [see inset 2(a)], indicate a perfect and atomically flat crystalline surface. During subsequent deposition of Y123, clear intensity oscillations are observed, which indicate 2D growth. Oscillations of the specular RHEED intensity are also observed during deposition of Y123 on double or TiO_2-terminated substrates, but the recovery is smaller than in the case of initial Y122 layer. Moreover, while clear 2D spots [inset 2(b)] are observed in the RHEED pattern of Y123 on Y122, on a DT-STO substrate [inset 2(c)] only streaks can be seen. Both facts reflect that the surface step density and, therefore, the surface roughness increase when increasing the number of possible interface stacking sequences.

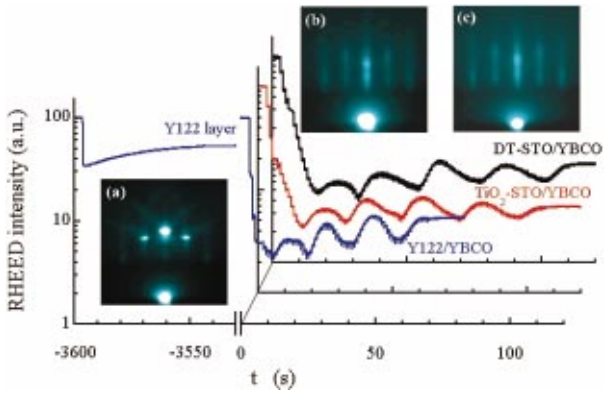

FIG. 2. (Color) RHEED intensity recorded during growth of Y123 ultrathin films with different control on the interface stacking: on a STO substrate with mixed SrO- and TiO_2-termination (named DT), on a single TiO_2-terminated one (named TiO_2) and when using an initial Y122 layer before the deposition of the Y123 (named Y122). In the insets the RHEED patterns are shown after: (a) the deposition of the initial Y122 layer, (b) and (c) the deposition of the Y123 on Y122 and on DT-STO, respectively.

In order to analyze the in-plane ordering and, subsequently, the network of antiphase boundaries, we have measured (00*l*)-rocking curves (ω-scans). In the inset of Fig. 3, (005)-rocking curves for Y123 grown on an initial Y122 layer and on DT-STO are shown. In both cases, the observed

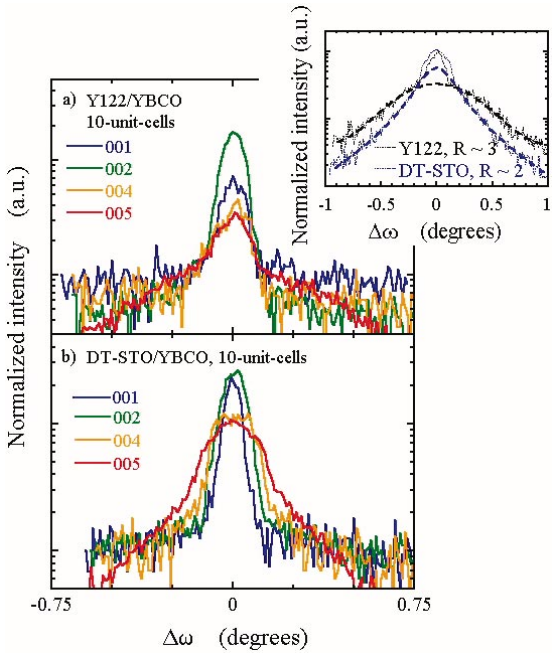

FIG. 3. (Color) Normalized (00*l*)-rocking curves (l=1, 2, 4, and 5) of Y123 films grown with an initial Y122 layer showing a constant angular width, indicative of rotational disorder (a) and on a DT substrate, where the main diffuse component broadens with l, indicating that also a shortening of the in-plane coherence length occurs (b). In the inset, the corresponding (005)-rocking curves are shown presenting the two component characteristics of weakly disordered systems.

shape exhibits two parts: a satellite (broad) component and a main peak (narrow component), which is characteristic for weakly disordered systems.[12] The δ-shaped coherent peak, related to perfectly aligned regions, cannot be resolved due to the resolution limitation of our apparatus. As can be seen from the inset, the line shapes of the broad components are different in both cases (Gaussian on an initial Y122 layer and Lorentzian on DT-STO), which has been previously attributed to different densities of APBs.[13] Moreover, on increasing the number of possible interfacial configurations the ratio between the intensity of the narrow and broad components (R) decreases. This is caused by the extension of the diffuse spots perpendicularly to the diffraction vector when increasing the defect density.[12] Further information on the disorder as a function of interface engineering can be obtained by comparing the ω scans of different (00l)-reflections. Lattice mismatched epitaxial layers such as the Y123 films can be considered as separated mosaic blocks on a substrate. In this picture, the diffuse component of the rocking curve is influenced by two main factors: slightly in-plane misorientation and small coherence length parallel to the substrate.[14] In Fig. 3(a), it is shown that the main peak of Y123 with an initial Y122 layer presents a constant lateral width in angle space, $\Delta\omega=\omega-\vartheta_1$, being ϑ_1 the position of the corresponding Bragg reflection, which is a clear indication of disorder of rotational nature.[13,14] Meanwhile, the film on DT-STO exhibits a width increase with l, as can be seen in Fig. 3(b), which means that the broadening of the rocking curve is related also to a shortening of the coherence length caused by a higher density of in-plane defects. All these observations support our idea that by controlling the SSI the density of antiphase boundaries can be modified.

Finally, Fig. 4 shows the normalized electrical resistance against temperature curves for 7-unit-cell-thick films with the three available interface configurations. It can be seen that there is a close relationship between the electrical properties and the density of APBs, controlled by the number of SSIs. It is shown that a higher density of APBs leads to a higher superconducting transition temperature, T_c, and a larger slope of the temperature dependence of the normal-state resistance. This behavior is attributed to the degree of oxidation of the YBCO ultrathin films, since these planar defects are supposed to favor oxygen in-diffusion in RE123 thin films, in a similar way as other defects, like dislocations, do.[15] An observation giving support to this idea is that after postgrowth oxidation treatment[16] of these films, T_c tends to approach the same value, as shown in Fig. 4. This indicates that the low concentration of defects in the film with the Y122 interface is the main cause for the oxygen deficiency and, therefore, the degraded superconducting properties observed in these as-made films. The diffusion of oxygen in the film is comparatively slower and requires longer oxidation times.

In summary, we presented a method of tuning the network of antiphase boundaries formed during the initial stage of RE123 films by reducing the number of possible atomic stacking sequences. A unique interface configuration is achieved by depositing the first unit cell layer with the cation ratio Y:Ba:Cu=1:2:2, instead of 1:2:3, on single TiO_2-terminated $SrTiO_3$. Control of the SSI has allowed us to study the influence of the density of APBs on the electrical transport properties of the superconducting film. We have found that the critical temperature T_c is depressed by increasing the in-plane ordering, which strongly indicates that the presence of APBs in the sample favors the oxygen in-diffusion and the relaxation of the in-plane strain.

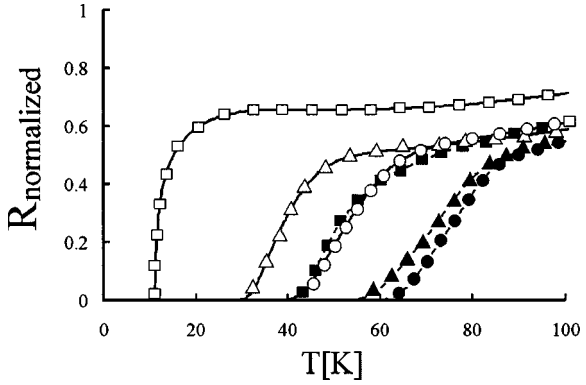

FIG. 4. Temperature dependence of the resistivity, $\rho(T)$, curves for 7-unit-cell-thick films with different degrees of control at the interface, i.e., Y122(□), TiO_2-termination (△), and DT (○). The closed symbols mark the resistivity after postgrowth oxidation treatment.

S.R.C. acknowledges financial support from the Spanish Ministry of Education.

[1] T. L. Hylton and M. R. Beasley, Phys. Rev. B **41**, 11669 (1990).
[2] B. Dam, J. M. Huijbrechtse, F. C. Klaassen, R. C. F. van der Geest, G. Doornbos, J. H. Rector, A. M. Testa, S. Freisem, J. C. Martinez, B. Stäuble-Pümpin, and R. Griessen, Nature (London) **399**, 439 (1999).
[3] M. McElfresh, T. G. Miller, D. M. Schaefer, R. Reifenberger, R. E. Muenchausen, M. Hawley, S. R. Foltyn, and X. D. Wu, J. Appl. Phys. **71**, 5099 (1992).
[4] T. Haage, J. Zegenhagen, J. Q. Li, H.-U. Habermeier, M. Cardona, C. H. Joos, R. Warthman, A. Forkl, and H. Kronmüller, Phys. Rev. B **56**, 8404 (1997).
[5] S. Bals, G. Rijnders, D. H. A. Blank, and G. van Tenderloo, Physica C **355**, 225 (2001).
[6] R. Ramesh, A. Inam, D. M. Hwang, T. S. Ravi, and T. Sands, J. Mater. Res. **6**, 2241 (1991); J. G. Wen, C. Træholt, and H. W. Zandbergen, IEEE Trans. Magn. **25**, 2418 (1993); B. Dam, C. Træholt, B. Stäuble-Pümpin, J. Rector, and D. G. de Groot, J. Alloys Compd. **251**, 27 (1997).
[7] G. Koster, B. L. Kropman, A. J. H. M. Rijnders, D. H. A. Blank, and H. Rogalla, Appl. Phys. Lett. **73**, 2920 (1998).
[8] See, e.g., L. X. Cao, T. L. Lee, F. Renner, Y. Su, R. L. Johnson, and J. Zegenhagen, Phys. Rev. B **65**, 113402 (2002).
[9] A. Abert, J. P. Contour, A. Defossez, D. Ravelosona, W. Schwegle, and P. Ziemann, Appl. Surf. Sci. **96–98**, 703 (1996), and references therein; L. X. Cao, J. Zegenhagen, E. Sozontov, and M. Cardona, Physica C **337**, 24 (2000).
[10] G. Koster, G. J. H. M. Rijnders, D. H. A. Blank, and H. Rogalla, Appl. Phys. Lett. **74**, 3729 (1999).
[11] G. J. H. M. Rijnders, G. Koster, D. H. A. Blank, and H. Rogalla, Appl. Phys. Lett. **70**, 1888 (1997).
[12] V. M. Kaganer, R. Köhler, M. Schmidbauer, R. Opitz, and B. Jenichen, Phys. Rev. B **55**, 1793 (1997).
[13] B. Dam, J. M. Huijbregtse, and J. H. Rector, Phys. Rev. B **65**, 064528 (2002), and references therein.
[14] P. F. Miceli and C. J. Palstrøm, Phys. Rev. B **51**, 5506 (1995).
[15] A. Kursumovic, P. Berghuis, V. Dediu, J. E. Evetts, F. C. Matacotta, and G. A. Wagner, Physica C **331**, 185 (2000).
[16] This postgrowth oxidation treatment was carried out in a tube oven using an oxygen pressure of 1 bar at 600 °C for 6 h and 450 °C for 18 h.